Review

Developments in PDT Sensitizers for Increased Selectivity and Singlet Oxygen Production

Nahid Mehraban and Harold S. Freeman *

Fiber & Polymer Science Program, North Carolina State University, Raleigh, NC 27695-8301, USA

* Author to whom correspondence should be addressed; E-Mail: hfreeman@ncsu.edu;
  Tel.: +1-919-515-6552; Fax: +1-919-515-3057.

Abstract: Photodynamic therapy (PDT) is a minimally-invasive procedure that has been clinically approved for treating certain types of cancers. This procedure takes advantage of the cytotoxic activity of singlet oxygen ($^1O_2$) and other reactive oxygen species (ROS) produced by visible and NIR light irradiation of dye sensitizers following their accumulation in malignant cells. The main two concerns associated with certain clinically-used PDT sensitizers that have been influencing research in this arena are low selectivity toward malignant cells and low levels of $^1O_2$ production in aqueous media. Solving the selectivity issue would compensate for photosensitizer concerns such as dark toxicity and aggregation in aqueous media. One main approach to enhancing dye selectivity involves taking advantage of key methods used in pharmaceutical drug delivery. This approach lies at the heart of the recent developments in PDT research and is a point of emphasis in the present review. Of particular interest has been the development of polymeric micelles as nanoparticles for delivering hydrophobic (lipophilic) and amphiphilic photosensitizers to the target cells. This review also covers methods employed to increase $^1O_2$ production efficiency, including the design of two-photon absorbing sensitizers and triplet forming cyclometalated Ir(III) complexes.

Keywords: photodynamic therapy; tumor selectivity; photosensitizer; polymeric micelles; singlet oxygen production; amphiphilic; drug delivery; nanoparticles; triplet photosensitizer

1. Introduction

Photochemotherapy of cancer is often called photodynamic therapy (PDT) [1]. PDT is a minimally-invasive treatment modality that has been shown effective for cancers characterized by early-stage superficial tumors, including lung, esophageal, gastric, and cervical cancers.

PDT has been used for cancer treatment since the 1990s utilizing Photofrin[®]. Some of the drawbacks with this first generation, FDA approved, PDT agent (a photosensitizer) are poor light absorption properties in the NIR region [2], skin sensitization as a side effect of PDT treatments, and the presence of a complex mixture of uncertain structures [3]. Consequently, the development of new PDT agents devoid of these shortcomings while meeting the vital criteria for PDT cancer treatment remains important. The PDT agents developed after Photofrin are known as second-generation PDT sensitizers and were the basis for our previous review [4]. The present review provides an overview of approaches to photosensitizer (PS) design for enhanced $^1O_2$ production and delivery for PDT as well as the fundamentals of this exciting technology.

1.1. Photosensitizers (PSs)

Dyes and pigments absorb and reflect certain wavelengths of light, which leads to the perception of color. Electronically, the difference between PS molecules and other dye types is the ability of PSs to transfer the energy of absorbed light to molecules in the vicinity or be utilized for photochemical reactions [5]. PSs are either porphyrin or non- porphyrin based. Examples of porphyrin-based PSs include phthalocyanines, chlorins, bacteriochlorin, and purpurins [4,6]. Protoporphyrin IX is a porphyrin based photosensitizers obtained from δ-aminolevulinic acid (ALA) through a biosynthesis mechanism [7].

Non-porphyrin based PSs include psoralens, anthracyclines, hypericin. hypocrellins, cyanines, phenothiazinium compounds such as methylene blue, Nile blue analogs, toluidine blue, rhodamines, triarylmethanes, and acridines [2]. Two of the most recent developed PSs are bodipy [8] and squarines [9]. Examples of the porphyrin and non-porphyrin based PS types are shown in Figure 1.

Key target criteria for PDT PSs include:

1. High selectivity toward cancer cells
2. Production of toxic reactive oxygen species (e.g., $^1O_2$) or free radicals
3. Optimal ADME (absorption, distribution, metabolism, excretion) [10]
4. Near IR light absorption
5. Absence of dark toxicity
6. High molar extinction coefficient

1.2. PDT Mechanism

PDT is based on the use of a PS, which efficiently populates an excited triplet state upon interaction with visible and NIR light. The triplet state of a PS (^{3}PS*) can produce toxic reactive oxygen species (ROS), such as $^1O_2$ or free radicals, by two different pathways. ^{3}PS* can react with molecules to generate intermediate free radicals that in turn generate ROS (type I photochemistry). Alternatively, it can directly interact with molecular oxygen in its ground triplet state ($^3O_2$) to produce *in situ* cytotoxic $^1O_2$ through an energy transfer process. This type II photochemistry (*cf.* Figure 2) is the most relevant PDT mechanism in cells, because most PSs are effective $^1O_2$ producers [11]. The ROS generated are capable of causing

irreversible damage if generated inside cells, particularly inside specific subcellular organelles (e.g., mitochondria) where PSs can localize and accumulate [11]. PDT would therefore be able to selectively kill diseased cells, provided that selective delivery of the PS to the target could be assured.
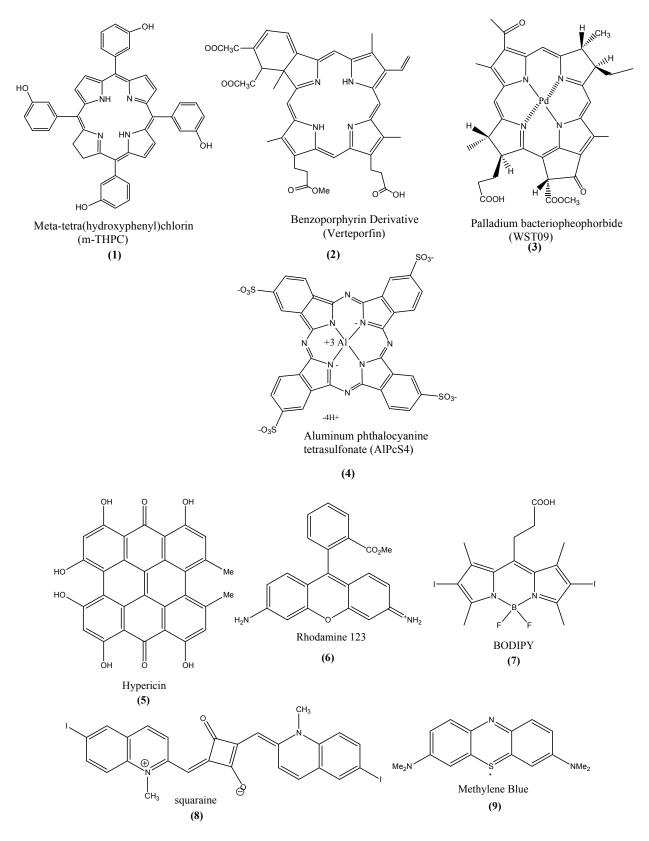
Meta-tetra(hydroxyphenyl)chlorin
(m-THPC)
(1)

Benzoporphyrin Derivative
(Verteporfin)
(2)

Palladium bacteriopheophorbide
(WST09)
(3)

Aluminum phthalocyanine
tetrasulfonate (AlPcS4)

(4)

Hypericin
(5)

Rhodamine 123
(6)

BODIPY
(7)

squaraine
(8)

Methylene Blue
(9)

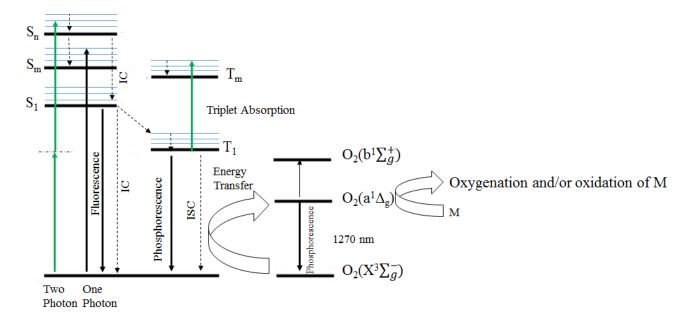**Figure 1.** Examples of porphyrin (**1**–**4**) and non-porphyrin (**5**–**9**) PSs.

Figure 2. Formation of PDT reactive species through type I and type II photochemistry (modified from [12]).

1.3. Singlet Oxygen Formation

The term singlet oxygen ($^1O_2$) refers to the two lowest energy excited electronic states of oxygen, $O_2(a^1\Delta_g$ and $O_2(b^1\sum_g^+)$, as shown in Figure 2. $O_2(b^1\sum_g^+)$ is unstable in aqueous media, decaying rapidly to $a^1\Delta_g$ [13]. One way to form $^1O_2$ involves energy transfer from an excited PS to ground state oxygen $O_2(X^3\sum_g^-)$. Energy transfer can also result in the production of $O_2(b^1\sum_g^+)$ which quickly decays to $O_2(a^1\Delta_g)$ in solution. $^1O_2$ can form upon oxygen quenching of the S_1 or T_1 state of the PS but the most efficient $^1O_2$ precursor is T_1, which has a longer lifetime than S_1 [12]. In general, the quantum yield of photosensitized singlet oxygen can be stated as:

$$\phi_\Delta = S_1 \text{ quenching} + T_1 \text{ quenching} \tag{1}$$

where S_1 quenching reflects the amount of $^1O_2$ produced by ground state oxygen quenching of the PS S_1 state and T_1 quenching reflects the amount of $^1O_2$ produced by quenching of the PS T_1 state [14].

A detailed and excellent discussion of the lifetime of intracellular $^1O_2$ is given in the review of Ogilby [12]. A critical point is that data from single cell and ensemble studies indicate that $^1O_2$ lifetime in a cell is significantly longer than long believed. Early on, time-resolved or photobleaching experiments were used to estimate intracellular $^1O_2$ levels and gave values of 10–300 ns [11,15–17]. Since then, the development of methods for monitoring $^1O_2$ from laser-induced phosphorescence, in time-resolved solution-phase experiments, led to lifetimes in H_2O and D_2O-incubated cells of ~3.5 μs and ~15–20 μs, respectively [17–19]. Clearly these values are much longer than long presumed.

Diffusion of $^1O_2$ through surrounding medium can take place once $^1O_2$ forms at sites where PS is localized. The distance, d, that $^1O_2$ subsequently travels has been estimated from the following equation:

$$d = \sqrt{6tD} \tag{2}$$

Thus, d depends on $^1O_2$ lifetime τ_Δ, the magnitude of diffusion coefficient D and time period t. Bearing in mind that $^1O_2$ lifetimes of 2–3.5 μs in H_2O and H_2O incubated cells, t = 5τ_Δ (10 μs) and a value of

4×10^{-6} cm^2 s^{-1} for D were used to estimate the radial diffusion distance [12]. This led to d = 155 nm. At τ_Δ ~25 µs, d = 550 nm was obtained. These results indicate that the long accepted diffusion limit of 10–20 nm from the site of ^{1}O$_2$ formation is no longer appropriate.

1.4. Mechanisms of Cell Death

While dependent on many factors, with the subcellular location of the PS being only one, PDT treatment can cause cell death by pathways involving apoptosis and necrosis. Necrosis is an unprogrammed cell death that is caused by chemical and physical damage [20]. It is a quick method of degradation that can affect widespread cell populations and can be characterized by cytoplasm swelling, damage to organelles, and disruption of the cell membrane. As a result of necrosis, intracellular contents will be released which leads to inflammation *in vivo*. Necrosis is more likely to happen when high doses of light are being used. Apoptosis is a programmed cell death that can be identified in single cells that are surrounded by other normal-looking cells and is characterized by cell shrinkage. Apoptotic cells tend to fragment into multiple membrane enclosed spherical vesicles, *in vitro*. These vesicles can be scavenged by phagocytes *in vivo*, and inflammation can be prevented in case of apoptosis and cells die in an immunologically-controlled way. [20]. Recent studies have shown that autophagy plays a role in PDT [21]. Autophagy is a process involving the transportation of cellular organelles and proteins through lysosomal degradation pathways and is related to cell survival, development, and differentiation. When proteins undergo irreversible ROS damage forming toxic oxidized protein, autophagy will be stimulated to remove these toxic species. Failure in these mechanisms leads to accumulation of oxidized macromolecules beyond the capacity of the cell to be repaired. In this case, the vital functions of the cells will be compromised which leads to cell death [22].

PSs differ in terms of pharmacokinetics and biodistribution. After their injection into the blood stream, they can bind to endothelial cells, the adventitia of the vessels, then accumulate within the tumor cells or bind to the extracellular matrix. The cytotoxicity induced by the absorbed light is restricted to the area of irradiation [23]. The effectiveness of PDT depends on the stage at which light has been delivered [24]. PDT can also lead to tumor death by deprivation of oxygen and nutrition arising from anti-vascular effects such as hemorrhage or thrombosis in tumor blood vessels [24].

1.5. Therapeutic Irradiation

To avoid undesired light absorption by biological chromogens instead of the PSs, the λ_{max} of the target PS should be >650 nm. Excitation at wavelengths in the near IR region also leads to deeper light penetration. This range of wavelengths is called the therapeutic irradiation window and is illustrated in Figure 3 [25]. Bearing in mind that the energy of the light decreases as wavelength increases, the preferred λ_{max} has been reported to be 630–800 nm by some [16] and 650–950 nm by others [26]. The molar absorptivity (ε_{max}) of a PS should be >20,000 to minimize the required dose of the PS for PDT treatment [27].
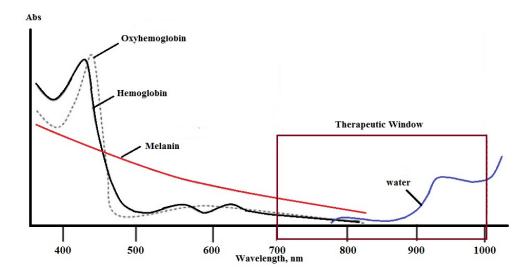
Figure 3. Illustration of the therapeutic window for PDT treatment.

1.6. Importance of Subcellular Localization

Controlling the subcellular localization of PS in cells is important because this has an impact on both PDT efficiency and the potential for cytotoxic affects. In this regard, it has been reported that even low levels of singlet oxygen generated in or near the mitochondria is far more efficacious than a large amount generated in the cell nucleus [28]. This opens the door to a pro-drug approach, *i.e.*, forming the PDT-active species at the target site, as an ideal way to minimized unwanted cytotoxic activity. An example is the formation of PpIX from ALA (5-aminolevulinic acid) in the mitochondria. It should be noted, however, that localization of PS in a subcellular structure does not guarantee that it will remain there. Depending on PS solubility and local concentration gradients it can diffuse out to the cytoplasm. Consequently, the design of PSs capable of bonding to the target site has been suggested [22].

It is also reported that low-level lysosomal photodamage can increase PDT efficiency due to subsequent mitochondrial photodamage. This phenomenon is not related to the amount of ROS formation, but appears to involve an increase in apoptotic signals arising from mitochondrial photodamage [29]. Localization of PS in mitochondria can be observed by using fluorescence imaging to monitor the coincidence of the PS and Rhodamine-123, taking advantage of the utility of Rhodamine-123 as a mitochondria specific stain. Examples of PSs targeting lysosome and mitochondria are listed in Table 1.

Table 1. Examples of PSs targeting lysosome and mitochondria.

Photosensitizer Type	Sub-Cellular Localization	Reference
N-aspartyl chlorin E6 (NPe6)	Lysosome	[29]
(Benzoporphyrin derivative) (BPD)	Mitochondria	[29]
5-Ethylamino-9-diethylaminobenzo [a]phenothiazinium chloride (EtBNS)	Lysosome	[29]
Galactose conjugate of 3-(1-hexyloxyethyl)-3- devinyl pyropeophorbide-a (HPPHgal)	Lysosome	[29]
Porphyrin-rhodamine B cation	Mitochondria	[30]
Porphyrin-mono-triphenyl phoosphonium cation	Mitochondria	[30]
Triphenylphosphonium (TPP) cation	Mitochondria	[31]
(E)-*N*-alkyl-4-[2-(ferrocenyl) vinyl]pyridinium cations	Mitochondria	[31]

Relatively new PS compounds targeting mitochondria include Zn(II) *N*-alkylpyridylporphyrins Figure 4. The presence of *n*-hexyl groups in these cationic compounds increased mitochondrial uptake and distribution. Localization in the vicinity of cytochrome c oxidase caused its inactivation during illumination. Light-induced inactivation accounts for the resultant mitochondrial photodamage and suppressed respiration and cell death [32].
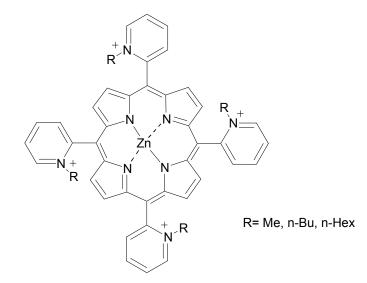

Figure 4. Structure of Zn(II) *N*-alkylpyridylporphyrins designed for mitochondria targeting.

2. PS Uptake and Selectivity

While the formation of $^1O_2$ in the right subcellular location is essential to optimizing PDT efficiency, the proficient delivery of PSs to the right location is the essential starting point. Key considerations associated with achieving this goal are covered in this section.

2.1. Effect of Hydrophobicity (Lipophilicity) and Hydrophilicty on Cell Uptake and Selectivity

Arguably, one of the most critical issues in PDT sensitizer design is selectivity. The higher the selectivity, the higher the accumulation of the PS in cancer cells and the lesser the side effects for patients. PS selectivity is influenced by its hydrophobicity/hydrophilicity and can be expressed as the logarithm of the octanol/water partition coefficient (logP) as well as the degree of asymmetry that is present in the PS. Typically, a molecule with average size of the porphyrin, 2,3-dihydroxy-5,10,15,20-tetrakis(3-hydroxyphenyl) porphyrin, with logP of 9.3 can enter the cells upon diffusion through the phospholipid bilayer [33].

Most of the relatively hydrophobic PSs show sufficient affinity to bind to membranes. Even water soluble PSs such as *N*-aspartyl Chlorin e6(NPe6) and sulfonated porphyrins/phthalocyanines bind to the membrane because they also contain a large hydrophobic ring [34]. An example of an amphiphilic PS that accumulates in lysosomes and endosome *in vitro* and *in vivo* is AlPcS2a [15] and an example of a lysosomal PS is *N*-aspartyl chlorin e6 (NPe6). It has been demonstrated that PDT using lysosomal NPe6 on living human cell lung adenocarcinoma cell (ASTC-a-1), initiated a mitochondrial apoptotic pathway [35]. Temopofin, known by brand name of Foscan®, is a lipophilic sensitizer with logP of 5.5 that tends to aggregate and interact with plasma proteins [10] and cell membranes [36].

Hydrophilic as well as aggregated PSs will be taken up through pinocytosis and/or endocytosis and they will accumulate mostly in the lysosome and endosome. As a consequence of light exposures, lysosomes become permeabilized and the sensitizers and enzymes can be released into the cytosol. As a result, tubulin forms which leads to accumulation of cells in mitosis and causes cell death in some cases [37]. Accumulation of cationic PSs takes place mostly in mitochondria because of the transmembrane potential of the inner mitochondrial membrane [38]. Cationic PSs with a delocalized positive charge tend to localize in mitochondria with a high negative membrane potential of 150–170 mV [31].

One advantage of hydrophilic PSs is their low tendency to aggregate in aqueous media. Aggregation facilitates internal conversion to the ground state which suppresses ISC [39]. Another advantage of hydrophilic PSs is that they decompose or disappear from the body faster, which results in fewer side effects. Consequently, water solubility can increase bioavailability and *in vivo* distribution [40]. The disadvantage of hydrophilic PSs is the low penetration of these compounds through cell membranes compared to hydrophobic PSs. AlPcS is an example of a hydrophilic PS having low cell internalization efficiency [41]. Water soluble phenothiazinium compounds such as methylene blue not only have poor cell/tissue penetration, they also have low stability under reductive biological conditions [42].

Although hydrophobic (lipophilic) PSs have a higher tendency to permeate cell membranes, their tendency to undergo aggregation in aqueous media makes them non-ideal without using a suitable delivery system. Hydrophobic PSs also tend to remain longer in the patient's body compared to hydrophilic PSs. These observations have caused PSs with amphiphilic properties through conjugation with water soluble or amphiphilic polymers or colloidal administrations to become attractive in PDT studies [43–47].

2.2. Effect of Intracellular pH on PS Uptake

PS uptake into various organelles is also affected by internal pH. It is known that the pH of organelles such as the Golgi apparatus, endosomes, and lysosomes are 6.7, 6.5, and 5.5, values that are lower than the pH of the cytosol and mitochondria (7.2–7.5) in normal cells. In addition, it has been reported that the pH of some types of cancer tissues are in the slightly acidic range, viz. < 7.3. Interestingly, there are few examples of reversible on/off pH-probes that respond to changes in intracellular pH. Regarding pH probes that are sensitive to a change in intracellular pH, Ir-tolylpyridine complexes have been used to selectively stain lysosomes. For instance, a new pH-sensitive Ir(III) complex was developed that contains three *N,N*-diethylamino groups (Figure 5). The luminescence emission of the complex produced a band at 554 nm in DMSO, which was ~60 nm shorter than the analog having $R = NH_2$. Protonation of the three NEt_2 groups induced a considerable enhancement in the band at 497 nm. In aqueous media, the emission intensity of this complex at 494 nm was very weak at pH > 7.4 but was considerably enhanced at pH < 7. In a subsequent study, new pH-responsive Ir(III) complexes were developed, leading to $^1O_2$ generation upon irradiation. The induction of necrosis-like cell death of HeLa-S3 cells upon irradiation of at 465 nm was reported [48,49].
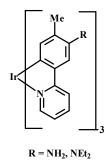
R = NH₂, NEt₂

Figure 5. Examples of pH responsive Ir(III) complexes.

2.3. Use of Nanoparticles

One approach to increasing PS selectivity involves using a molecule having high affinity toward cancer cells, such as folic acid [50,51] or antibodies [52], peptides, LDLs, and polymers [3]. This approach is employed for third-generation PSs wherein the affinity for cancer cells increases by targeting subcellular compartments such as mitochondria [53]. Therefore, third-generation PSs are often second-generation PSs bound to carriers for selective accumulation in tumors [54].

The second approach involves using nanoparticle-based drug delivery methods in PDT. Although amphiphilic PSs or third-generation PSs can enhance selectivity, employing nanoparticles in PDT studies has become very attractive for the following reasons: (1) lower levels of the PSs can be used for PDT treatment; (2) PSs can be used in monomeric form within some of the nanoparticles; (3) most of the FDA approved PDT agents are hydrophobic and nanoparticles can increase the selectivity of these compounds to reduce side effects after treatment as well as aggregation problems; (4) dark toxicity would be less of a problem [55]; (5) exploiting strategies such as pH sensitivity, thermal sensitivity, peptide or antibody tags in nanoparticle system can increase selectivity more efficiently; (6) having control on making nanoparticles with a diameter of less than 200 nm for better passive targeting through EPR system; (7) increase in cell uptake [38,46]. Examples of some of the nanoparticles that have been used in PDT studies so far include liposomes [56,57], micelles, polymeric micelles, carbon nanodots [58], quantum dots, catanionic vesicles [59], gold nanoparticles [60,61], hydrogels [62], and dendrimer nano particles [63], TiO₂ [64], examples of which are shown in Figure 6.
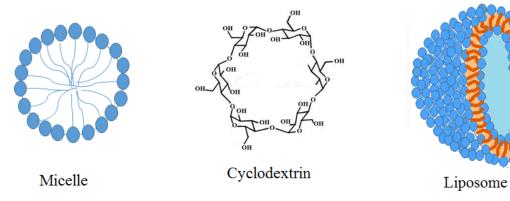

Micelle
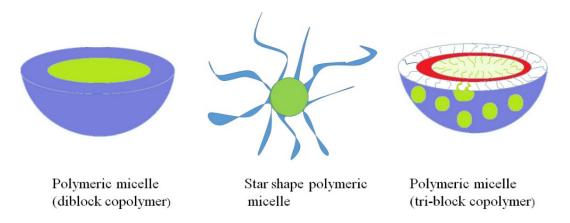
Cyclodextrin

Liposome

Figure 6. *Cont.*

Figure 6. Examples of nanoparticle structures developed for PDT treatments.

Polymeric Micelle/Micelles

Polymeric micelles are made of amphiphilic block or graft copolymers that form spontaneously in aqueous media due to thermodynamically-favored aggregation above the critical micelle concentration (CMC) [65]. Micelles with lower CMC levels have higher thermodynamic stability, which can be obtained by increasing the hydrophobic section of the amphiphiles [65,66]. Below the CMC level polymer chains tend to remain in the monomolecular state. As their concentration in water increases, however, the hydrophobic component tries to escape water and forms the inner core. Subsequently, the hydrophilic head interacts with water on the surface of the spherical micelle and forms the corona. Formation of the micelle core is due mainly to hydrophobic interactions as well as hydrogen bonding of constituted block copolymer, metal complexation and electrostatic interactions [67]. A feature of polymeric micelle is illustrated in Figure 7.
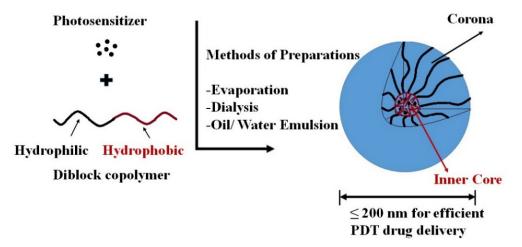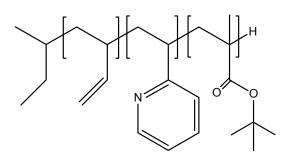

Figure 7. Schematic representation for spherical polymeric micelle formation via different methods. Co-solvent evaporation [68], dialysis [69], oil/water emulsion.

Having the hydrophobic core enables micelles to entrap hydrophobic PSs via secondary valency forces or electrostatic interactions. The use of nanoparticles such as polymeric micelles provides the framework for next generation PSs [70]. In addition to di-block copolymers, tri-block copolymers, Figure 8 [71], star-shaped polymers [68,72] can be used to form micelles. In some cases the polymer component is a polypeptide [73].

polybutadiene-block-poly(1-methyl-2-vinyl pyridinium methyl
sulfate)-block-poly(methacrylic acid) (BVqMAA) triblock terpolymers

Figure 8. Examples of tri-block copolymers used to form polymeric micelles.

Studies in this area have taken into consideration that the PS employed may concentrate in the tumor cells via active and passive-targeting strategies [74]. Using artificial carriers such as cationic liposomes, silica nanoparticles, and polymeric conjugates can prolong the plasma circulation half-lives of the PS and increase its accumulation in tumors through enhanced permeability and retention effects [74,75].
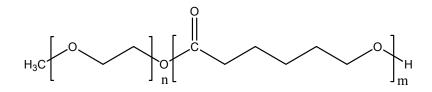
The passive targeting mechanism takes advantage of an "enhanced permeation and retention" (EPR) process. EPR allows preferential extravasation of drugs though leaky vasculatures, due to having an incomplete endothelial barrier and poor lymphatic drainage in most of the tumor structure [76,77]. Stimuli-responsive polymeric micelles giving controlled release upon pH and temperature changes can be used to increase PS delivery to the specific target [78]. Salt concentration, magnetic fields, light [71], chemical auxiliaries, and enzymes [79,80] are types of stimuli than can be used. In addition to the EPR mechanism, active targeting facilitates penetration of the PS carrier into the cancer cells via surface functionalization of the nanocarrier with a specific molecular motif such as an antibody or peptide. EGFR-targeting peptide ligand GE11 has been used to target head and neck squamous cell carcinoma H&N SCC cells *in vivo* and *in vitro* [76]. Active targeting prevents one of the problems associated with passive targeting, which is nanoparticles accumulated in the tumor stroma passively can be redistributed into the blood stream, which reduces selectivity [81].

One of the advantages of polymeric micelles over standard micelles made from compounds such as polysorbate 80 (Tween 80®) is their higher stability in solution. Also, polymeric micelles can solubilize a larger amount of the PDT agent and they are suitable for parenteral administration [65]. Micelles can be made of amphiphilic peptides. These amphiphiles can form spherical to nanofiber structures due to hydrogen bonding and hydrophilic interactions. Using lysine as a sub-unit, the hydrophilic component will be ionized at acidic pH levels and the micelles become destabilized due to electrostatic repulsion interactions [80].

Other advantages of polymeric micelles include ease of preparation, efficient drug loading, controlled drug release, and extended blood circulation that allows efficient targeting through the EPR effect. This also reduces the undesirable bio-distribution of hydrophobic compounds [82]. Polymeric micelles are one of the nanocarriers that can resolve the hydrophobicity and/or toxicity drawbacks of many PSs [73]. Polymeric micelles with diameter size of 10–200 nm can be used for drug delivery because they are large enough to escape rapid renal clearance and small enough to avoid removal by reticuloendothelial clearance (RES). Therefore, permeability and retention (EPR) in tumor tissue will take place more effectively in

vascular architecture that is leaky or defective around tumor cells [70,78]. Usually the hydrophilic end of the molecule is PEG and this forms small size micelles (10–100 nm) [83].

One drawback of having long circulating polymeric micelles is unwanted photoactivity in normal cells. Li and co-workers showed that PEG-b-PCL, Figure 9, containing a generator and scavenger of $^1O_2$ combination can reduce phototoxicity in normal cells [82].

Poly(ethylene glycol)-b-poly(caprolactone) (PEG-b-PCL)

Figure 9. Structure of PEG-b-PCL.

To increase the inherent biocompatibility and bioactivity of micelles, peptides can also be used. The problem with these types of micelles is a low hydrophobic tail interaction that decreases the stability of the micelles. This problem can be resolved by increasing the number of hydrophobic tails. Formation of a stable micelle is achieved by utilizing a surfactant-like amphiphilic peptide, Figure 10, with four hydrophobic tails [84].
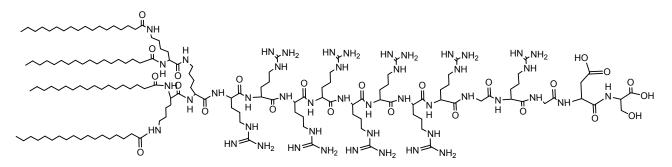

Figure 10. Structure of a surfactant-like tetra-tail amphiphilic peptide.

Another advantage to using polymeric micelles is the ability to protect unstable PSs such as 5-ALA in aqueous media at neutral to basic pH. 5-ALA is a pro-drug that can be converted into protoporphyrin IX (PpIX) in proliferating cancer cells *versus* normal cells. 5-ALA is also very polar, which limits its diffusion through membranes. Conjugation of PpIX to PEG-PLA, Figure 11, increases PDT efficiency [85]. Hydrophobic PS conjugated to hydrophilic polymers can self-assemble into nanoparticles [86].

Controllable release is another advantage of using polymeric micelles. Trigger-controllable release of the PDT sensitizer by L-phenylalanine was reported for biodegradable supramolecular polymer micelles (SMPMs). In response to an additional L-phenylalanine molecule, SMPMs disassemble due to interactions between L-phenylalanine and sensitizer-loaded SMPMs [87]. To increase the stability of the polymeric micelles nanoparticle, it can be mineralized using calcium phosphate [73].

One way to influence sensitizer release from polymeric micelles is to take advantage of the pH difference between the extracellular of normal cells *vs.* tumor tissue. The extracellular pH of tumor tissue is typically 6.4–6.8, due to accumulation of lactic acid [88], while the extracellular pH is 7.4 for normal cells. However, only a few pH-sensitive polymers are responsive to the extracellular pH of tumor tissue

and others are sensitive to endosomal or lysosomal pH. pH-Responsive MPEG poly(β-amino ester) polymeric micelles are responsive to extracellular tumors. This type polymer micelle is pH responsive due to its tertiary amines [78], an example of which is shown in Figure 12.
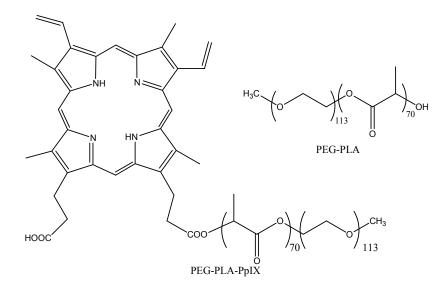

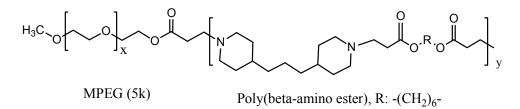**Figure 11.** Conjugation of protoporphyrin IX to PEG-PLA.

Figure 12. A pH sensitive MPEG poly(β-amino ester) structure for micelle formation.

Some of the recent studies involving the use of polymeric micelles are summarized in Table 2, and examples of polymer structures are shown in Figure 13.

Utilizing DSPE-mPEG$_{2000}$ micelles, 89% of hypericin was encapsulated and sub-localization into mitochondria occurred. Phototoxicity increased 2.5-fold compared to the case involving PEGylated PSs [89]. Drug loading efficiency for MPEG-poly(β-amino ester) block copolymer of 70%–80% was reported for PpIX [78]. Using PEO$_{750}$-b-PCL5 polymer increased the cell uptake by 60% for phenophobide [70]. Loading capacity of encapsulated PpIX will increase from 0.2% to 4% by conjugation of the PpIX with PEG-PLA [85]. Highest loading capacity was observed using micelles containing benzoyl and naphthoyl end groups. The loading capacity for these micelles was 30% w/w [83]. Phototoxicity of dendrimer phthalocyanine encapsulated in PEG-PLL increased by 100-fold compared to the dendrimer phthalocyanine itself, Figure 14 [90].

Many studies using nanomedicine technologies have been conducted. However, translating these studies into clinical application will not be possible if the parameters needed to maximize cell killing were not reported. As an example, optimized or maximum cell internalization is reported as ≤ 2 h for A431 cells and takes place when a 10 mol% EGFR-PEG-PCL-GE11 component is used in micelle formulation [91].
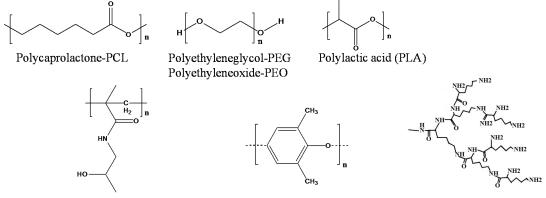
Table 2. Examples of polymeric micelles/micelles tested *in vitro* and *in vivo* for PDT.

Strategy for Targeting & Drug Release	Sensitizer	Polymer/Monomer	Loaded Particle Size (nm)	*In vitro*/*In vivo*	Ref.
Active targeting	Silicon phthalocyanine	PEG-PCL-GE11 Peptide (YHWYGYTPQNVI)		Human epidermoid carcinoma and head & neck cancer	[76,81]
Active targeting Folate amino acid and overexpressed folate receptor	THPC	Poly (2-ethyl-2-oxazoline)-*b*-poly(d, l-lactide) (PEOz-PLA) (m-THPC-PM) (folate-m-THPC-PM)	103.8	*In vitro* on epidermoid cell line (KB); *In vivo* on KB xenograft mice	[78,92]
Active Galactosyl moiety for increased selectivity toward ASGP receptors on HepG2 cells	Porphyrin (conjugated to polymer)	APP-PAEMA_PCL Gal-APP-PAEMA-PCL	60	Human laryngeal carcinoma (HEp2); Human hepatocellular liver carcinoma (HepG2)	[69]
Passive Cellular endocytosis	Doxorubicin (DOX)	Star shaped poly(L-lysine) dendrons porphyrin polymer (PP-PLLD)	150–192.5	Human nasopharyngeal carcinoma (CNE2)	[72]
Passive targeting; Dual chemo-photodynamic therapy	Paclitaxel Synthetic chlorin	Star-shaped di-block copolymer (CSBC-58)	103.2	Breast cancer (MCF7)	[68]
Passive targeting	Pheophorbide a (phA) & β-carotene(CAR)	Poly(ethylene glycol)-b-poly(caprolactone) PEG-b-PCL	100	Human breast and cervical cancer cell line	[82]
Passive targeting	Chlorin e6	Poly(ethylene glycol)-b-poly(l-aspartic acid)-b-poly(l-phenylalanine) (PEG-PAsp-PPhe)	74.6	*In vitro* assay on MCF7	[73]
Passive targeting (endocytosis); Dual chemo-PDT	*m*-THPC SN-38	Chlorinated core star shape block copolymer (CSBC)	115.7–163.7	Human colon cancer (HT-29); *In vivo* xenograft	[77]
Passive targeting Dual photothermal (PTT) and PDT	IR825 Chlorin e6	C18PMH-PEG-Ce6-Gd	100–200	*In vitro* and *in vivo* assay on 4T1 Cell line	[93]
Passive endocytosis	Dendrimer phthalocyanine DPc	DPc + (PEG-PLL) → (DPc/m)	50	A549 cells in mice	[90]
Passive targeting Accumulate in mitochondria	Hypericin	DSPE-mPEG$_{2000}$ micelle	12	Malignant brain tumor (MBTs)	[89]
Enzyme control release (in presence of L-phenylalanine)	THPP	Ethyl cellulose-graft-poly(ε-Caprolactone) and alpha cyclodextrin → EC-g-PCL and α-CD	205	85% THPP release in 6 h; MCF-7	[87]

<div align="center">

Table 2. *Cont.*

</div>

Strategy for Targeting & Drug Release	Sensitizer	Polymer/Monomer	Loaded Particle Size (nm)	*In vitro/In vivo*	Ref
Passive pH responsive polymeric micelles	PpIX	MPEG-Poly(β-amino ester) block copolymer (PpIx-pH-PMs)	122	*In vivo* on live SCC7 tumor-bearing mice; *In vitro* on SCC7 cells	[78]
Passive targeting	Pheophorbide	PEO$_{750}$-b-PCL5 polymer	20	Human breast cell line (MCF-7)	[70]
Passive targeting	Porphyrazine	Polybutadiene-block-poly(1-ethyl-2-vinyl pyridinium methyl sulfate)-block-poly(methacrylic acid) (BVqMAA) triblock terpolymers	256	*In vitro* assay on A549 cells; Diameter size 6%–12% loading; *In vivo* assay	[71]
Passive targeting	Chlorin e6/Fe$_3$O$_4$	Multimeric grain-marked micelles with Fe$_3$O$_4$ inner core and outer multi grain micelle PLLA-b-PEG-Ma	98	KB tumor-bearing nude mice *in vivo*; KB cells line *In vitro*	[94]
Passive targeting	PpIX	PEG-PLA	30	H2009 lung cancer cells	[85]
Polymer degrades at site of action due to presence of lipase	*m*-THPC	mPEG750-b-oligo(ε-caprolactone)5 (mPEG750-b-OCL5) with a hydroxyl, benzoyl or naphthoyl end group		*In vivo*; *In vitro* on head & neck squamous carcinoma cell line UM-SCC-14C	[83]
Study the effect of the length of hydrophobic units, PPO, on phototoxicity and solubility	ZnPc	Poloxamine polymers: T304 (15-PEO unit, 17.1-PPOunit) T904 (60.9-PEO unit, 69.3-PPO unit) T1107 (238.6-PEO unit, 77.6-PPO unit) T1307 (286.4-PEO unit, 93.1-PPO unit)	2.7 4.9 13.9 47.6	KB cells; Increase in phototoxicity and ZnPc solubility by increasing PPO unit	[65]
Passive targeting	Xanthene dye erythrosine B (ERY)	CTAB (cationic) micelle SDS (anionic) micelle		logP of 0.46 (hydrophilic dye)	[95]
Tri-block copolymer	Gn-DPcZn	Polyion micelle; Amphiphilic triblock copolymer; PLL-b-PEG-b-PLL		High stability *in vivo*	[96]
Passive targeting	Pheophorbide	PEO(2000)-b-PCL(2800) PEO(5000)-b-PCL(4000) PEO(2400)-b-PDLLA(2000) PEO(3100)-b-PS(2300)	20–30	HCT-116 human colorectal carcinoma	[97]

Figure 13. Examples of structural units reported in Table 2.

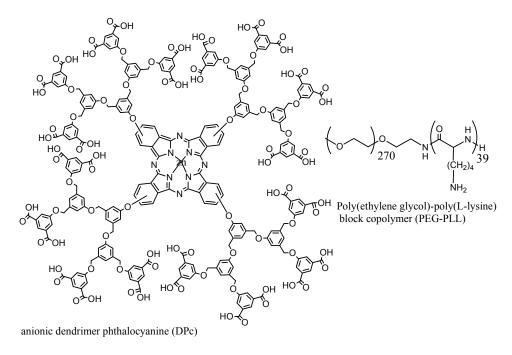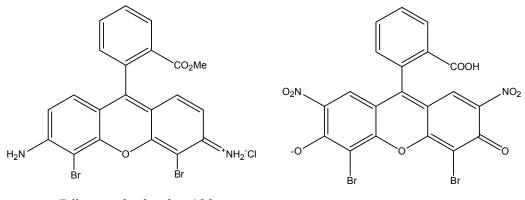anionic dendrimer phthalocyanine (DPc)

Figure 14. A dendrimer-based phthalocyanine structure for sensitizer delivery.

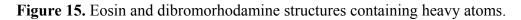## 3. Increased $^1O_2$ Production

3.1. Incorporation of Heavy Atoms

The ability to produce satisfactory levels of $^1O_2$ is a critical characteristic of PDT sensitizers and correlates with increasing the triplet excited state lifetime of a PS [98,99]. Increased triplet state lifetime can occur by increasing ISC efficiency. One way to increase ISC is by incorporating heavy atoms into the sensitizer structure, as illustrated for eosin and rhodamine in Figure 15 [100–102]. A closed-shelled diamagnetic metal is better suited than an open-shelled paramagnetic metal because the latter shortens the triplet lifetime and makes certain chromogens photo-inactive. Halogenation of the rings in the phthalocyanine (Pc) system, Figure 16, also increases the $^1O_2$ quantum yield, which can be explained using the principles of spin-orbit coupling. In this regard a bathochromic shift in absorption maxima as well as an slight increase in $^1O_2$ production was observed by substitution of H with halogens and follows the order of Cl < Br < I. Temperature, media viscosity, and oxygen concentration can also influence $^1O_2$
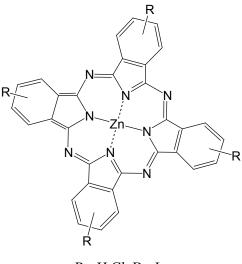
production [39]. The development of complexes contain Ir is another approach to increasing $^1O_2$ levels. For instance, cyclometalated Ir(III) complexes such as fac-Ir(ppy)$_3$ 1 (ppy = 2-phenylpyridine) and fac-Ir(tpy)$_3$ 2 (tpy = 2-(4′- tolylpyridine)) have unique photophysical properties as phosphorescence materials, since they possess high luminescent quantum yields and have relatively long phosphorescent lifetimes ($\tau \sim \mu s$) [49]. The highly efficient spin–orbit coupling of Ir(III) metal ion in the complexes promotes ISC to the triplet state. Consequently, these complexes exhibit strong phosphorescence even at room temperature. The authors also used DFT calculations to show that protonation of the pyridyl groups narrows the HOMO–LUMO energy gap and induces a red-shift in the emission wavelength [49].

Dibromorhodamine 123   Eosin

Figure 15. Eosin and dibromorhodamine structures containing heavy atoms.

R= H,Cl, Br, I

Figure 16. Halogenated Zn-Pc structures for enhanced $^1O_2$ formation efficiency.

Incorporation of Ag (III) into *N*-confused porphyrin (H$_2$N$_2$CP) can also increase the efficiency of $^1O_2$ generation, Figure 17, by increasing ISC efficiency to the triplet state [103]. Incorporating heavy metals in 5,10,15,20-tetrakis(pentafluorophenyl) porphyrin, Figure 18, increased $^1O_2$ quantum yield from 0.28 to 0.89 and 0.92 for Pd(II) and Pt(III), respectively [104].
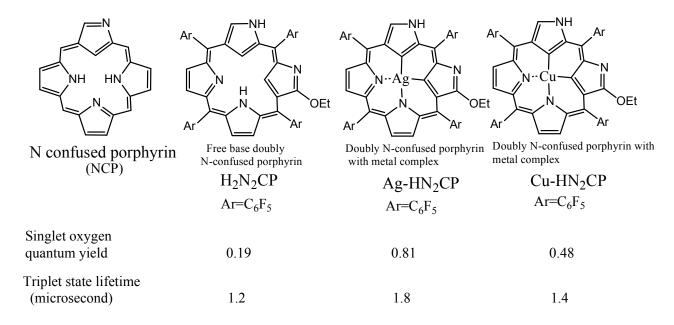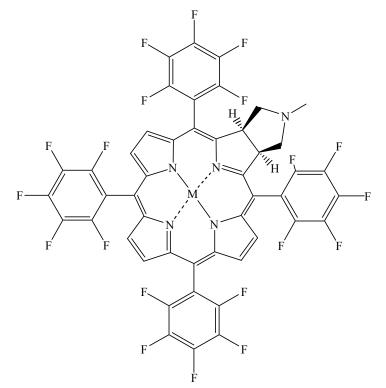
Figure 17. Properties of N-confused porphyrin (H₂N₂CP) with, and without, metal atoms.

M=2H, M=Pd, M=Pt

Figure 18. Pd- and Pt-complexed 5,10,15,20-tetrakis (pentafluorophenyl) porphyrin structures.

Up to a 70% increase in $^1O_2$ quantum efficiency was reported for Mg tetrabenzoporphyrin containing a pyridine ligand, Figure 19 [105]. Placing one or five Zn atoms into a picolylamine-based porphyrin raised the $^1O_2$ quantum yield from the 0.5 to 0.82 and 0.92, respectively [106].
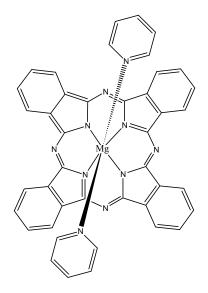
Figure 19. A Mg tetrabenzoporphyrin having high $^1O_2$ quantum efficiency.

3.2. Isosteric Replacements

Structures for enhancing intersystem crossing in polymethine-like molecules were developed, by replacement of oxygen atoms by sulfur in the squaraine system, as illustrated in the Figure 20. This replacement facilitates $S_1(n\pi^*)\rightarrow T_1(\pi\pi^*)$ and the magnitude of the resultant ISC rate constant increased $^1O_2$ quantum efficiency [107,108].
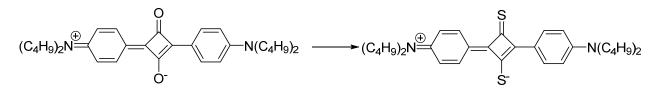

Figure 20. Modification of the squaraine system to increase $^1O_2$ quantum efficiency.

In the case of porphyrin and phthalocyanine systems, the conformation and the symmetry of these molecules also affects $^1O_2$ production [109]. In a study by Roder and coworkers, it was shown that the addition and the number of ethyl groups in tetraphenylporphyrins effected a gradual change in properties such as $^1O_2$ production and ISC. The ISC and $^1O_2$ quantum yield values for tetraphenylporphyrins with and without Zn are summarized in Figure 21. These measurements were conducted in DMF [110].

Incorporation of 1–4 bromine atoms into the porphycene macrocycle, Figure 22, changed $^1O_2$ efficiency from 0.36 to 0.9, 0.95, 0.71, and 0.49. It was also found that the symmetry and geometry of the molecules affected $^1O_2$ production [111]. Asymmetrical halogenated aniline-based squaraines, Figure 23, include an iodinated derivative giving increased $^1O_2$ production [112]. Molecules with higher symmetry have a similar singlet and ground state geometry. This similarity in geometry led to increased fluorescent quantum yield and reduced ISC efficiency.

$\varphi_{ISC, H2}$	0.72	0.68	0.63
$\varphi_{ISC, Zn}$	0.93	0.67	0.45
$\varphi_{\Delta, H2}$	1	0.94	0.83
$\varphi_{\Delta, H2}$	1	0.81	0.45

$\varphi_{ISC, H2}$	0.42	0.32	0.35
$\varphi_{ISC, Zn}$	0.62	-----	0.4
$\varphi_{\Delta, H2}$	0.13	0.11	0.32
$\varphi_{\Delta, H2}$	0.12	-----	0.24

Figure 21. $^1O_2$ quantum efficiency values for various tetraphenylporphyrins.

0.36   0.90   0.95

0.71   0.49

Figure 22. Brominated porphycene macrocycles and their $^1O_2$ quantum efficiency.

Singlet oxygen quantum yield
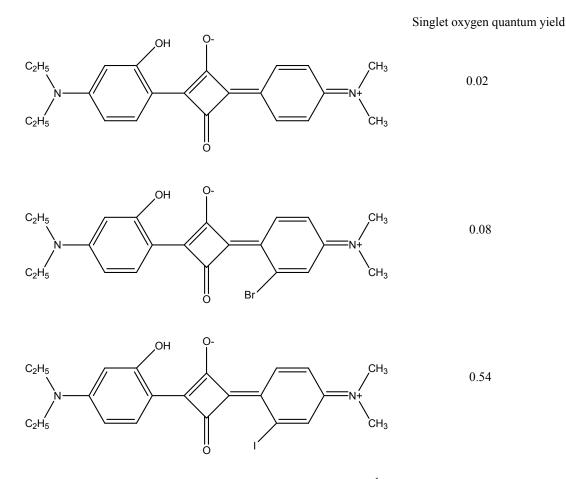

0.02

0.08

0.54

Figure 23. Iodinated squaraine giving enhanced $^1O_2$ quantum efficiency.

It is believed that the use of heavy atoms to encapsulate a PS enhances ISC and thus $^1O_2$ quantum efficiency. With this in mind, Pt(IV)- and Au-modified silica nanoparticles were developed as a delivery system for enhancing the PDT effectiveness of hypocrelin A (HA). Comparing $^1O_2$ efficiency results from encapsulating HA with, and without, Pt- and Au- modification, indicated that including one of these heavy atoms as a dopant increases $^1O_2$ generation [113].

Cyclometalated Ir complexes have grown in interest as PSs, due to recognition of their high quantum yields of triplet formation, long lifetimes of the excited triplet state (typically in the µs range), and triplet energy high enough to allow for the energy transfer process. Further, it has been shown that they are usually resistant to attack by $^3O_2$. However, disadvantages, such as low H_2O solubility, hinder biomedical applications of these complexes. To address this concern, the synthesis and photochemical characterization of a water-soluble Ir−PhenISA conjugate was undertaken, the results of which showed that binding to a suitable polymer improved the photophysical properties of the Ir emitters. In this regard, bis-(cyclometalated) Ir complexes appended to the polymer afforded triplet metal-to-ligand charge transfer excited states that can either radiatively decay or react with $^3O_2$ and can then be exploited for either imaging or PDT applications. It has been found that photoluminescence can be triggered by two-photon excitation, which offers advantages over traditional one-photon excitation in terms of less cellular damage and deeper light penetration *in vivo*. Specifically, binding an Ir(III) complex (triplet emitter) to a poly(amidoamine) gave the Figure 24 conjugate [11], doubling the luminescent quantum yield and demonstrating their potential use as both cell imaging agents and PSs for $^1O_2$ generation.
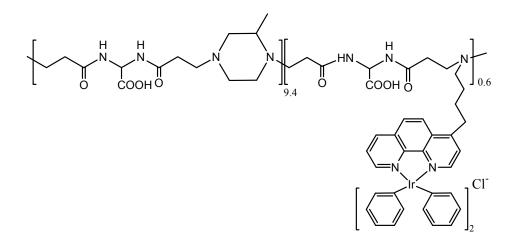
Figure 24. Poly(amidoamine) Ir(III) complex as a new $^1O_2$ sensitizer.

A group of water-soluble IR-bipyridyl complexes (Figure 25) displayed significantly reduced cytotoxicity, with half maximal inhibitory concentration (IC$_{50}$) values being up to 10^2 μM after a 48-h incubation, which were ~90 times larger than values from their PEG-free counterparts. It is believed that the reduced cytotoxicity originates from the PEG pendants, which prevent the complexes from interacting with intracellular DNA, proteins, and organelles [11,74,114]. The authors studied the photophysical and photochemical properties of their Ir(III) PEG complexes and their PEG-free counterparts and found that $^1O_2$ production efficiency was closely related to the emission lifetimes of the complexes, which can be systematically controlled by changing the cyclometalating ligands. The cellular uptake efficiency of the PEG complexes was lower than their PEG-free counterparts. Since all these PEG complexes were non-cytotoxic in the dark, but exhibited considerable light-induced cytotoxic activity, they have potential to serve as efficient PS for PDT. It was also confirmed that the PEG complexes were localized in the mitochondrial region, facilitating efficient oxidative damage of this cellular organelle and causing necrotic cell death upon light excitation [74].

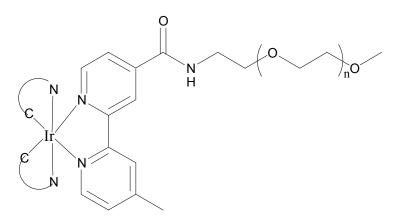**Figure 25.** Ir(III) PEG complexes as new $^1O_2$ sensitizer.

3.3. Two Photon Systems

Approaches to increasing triplet state efficiency include designing molecules capable of absorbing two photons simultaneously in the same quantum event. The associated electron donor (D) acceptor (A) combinations are linked through a conjugated linker (π-bridge) and are symmetrical or asymmetrical,

forming (D-π-D) or (A-π-A), (D-π-A)[115], (A-π-D-π-A) and (D-π-A-π-D) structures [116]. Two photon absorption (TPA) is very attractive for biological applications which require NIR absorbing systems [117]. One approach to increasing TPA efficiency is to incorporate a light-harvesting dendrimer (antenna) containing chromophores that funnel the excited-state energy of the PS without changing the desired photochemical and photophysical properties of the porphyrin, Figure 26 [117].

Two-photo activated PDT (2-γ PDT) provides the potential for treating deeper tumors and/or enhancing tumor targeting. Pyropheophorbide-a methyl ester (MPPa) has been used to study one- and two-photon activated PDT and it was found that femtosecond laser pulses at 674nm provides 1-γ PDT efficacy against cervical, lung, and ovarian cancer cells. It was also shown that MPPa can be activated by a 120 fs laser at 800 nm at a light dose causing no detectable phototoxicity [118].

Figure 26. A light harvesting dendrimer having fluorescence resonance energy transfer.

The addition of π-conjugation to Ru(II)-based PSs has been studied. The sensitizing ability of the complex increased by addition of one or two pyridine-quinoline hybrid systems to an anthracene unit. While the addition of two heteroaromatic ligands had a beneficial effect, adding a third group to the complex reduced photosensitization which is due to the bulkiness of the whole system, Figure 27 [119].

Figure 27. Structure of [Ru(LP1)₃][PF₆]₂.

3.4. Triplet PSs

Another approach to increasing ¹O₂ production involves the use of triplet PSs. Triplet PSs have applications in catalysis of organic reactions, light-induced hydrogen production, and PDT [120]. To produce a triplet PS, population of the first triplet excited state is required which can be done by ISC.
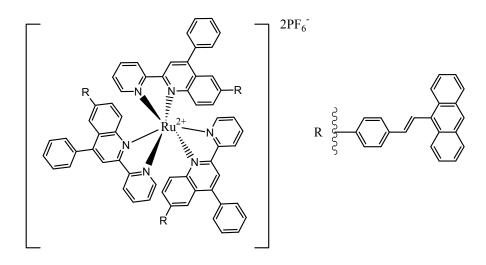
Cyclometalated Ir(III) complexes with styrylBODIPY ligands and showing NIR absorptions/emissions have been reported. The complexes were used as triplet PSs for ¹O₂ mediated photooxidations. In general, cyclometalated Ir(III) complexes having short absorption wavelength, weak absorption of visible light, and short-lived triplet excited states, are not suitable for PDT application PDT because strong absorption of visible light and long-lived triplet excited states are preferred [120,121]. Consequently, a key goal has been to develop new complexes that show strong fluorescence as well as satisfactory ISC. To develop transition metal complexes showing strong visible light absorption and long-lived triplet excited states bulky organic fluorophores have been attached to the coordination center using a C–C triple bond as the *p*-conjugation linker. In this way, the heavy atom effect of Ir(III) can be maximized and the excitation energy can be efficiently channeled to the triplet excited states thus enhancing the PDT applicability of Ir(III) complexes. More importantly, the absorption as well as the emission wavelengths can be extended to the NIR spectral region (644–729 nm). This approach led to heteroleptic cyclometalated Ir(III) complexes containing BODIPY (Figure 28) exhibiting strong NIR absorption, strong NIR fluorescence (700–800 nm), and long-lived triplet excited states (92–156 ms). The photophysical properties of the complexes and the NIR light-harvesting ligands were studied using steady state and time-resolved absorption/emission spectroscopy, as well as DFT calculations [122].

It has been reported that photooxidation enhancement can be accomplished through intramolecular resonance energy transfer (RET). In a study by Zhao and coworkers, Bodipy triad triplet PSs (Figure 29) were developed by connecting an unsubstituted styryl-BODIPY (energy donor), with λ_max of 409, to bisiodo aza-BODIPY (intramolecular energy acceptor) through click chemistry. The presence of additional absorption bands in the visible regions enhanced light absorption in the visible region. Therefore the energy of the donor can be transferred to the acceptor via ISC. Aza-BODIPY with a much larger absorption band functions as a spin convertor to produce the triplet excited state [123].
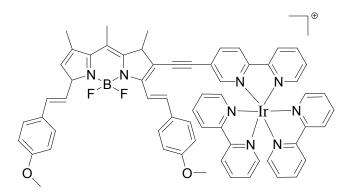
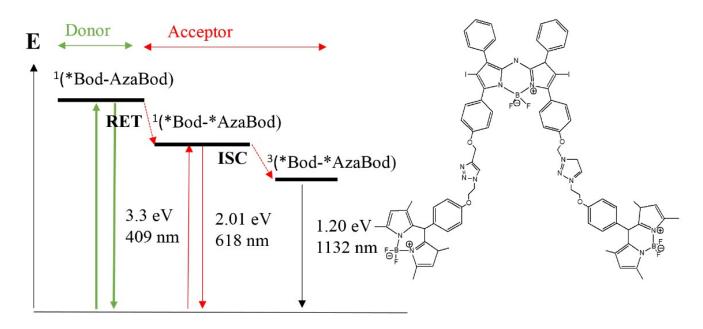**Figure 28.** Structure of cyclometalated Ir(III) complex.

Figure 29. Example of resonance energy transfer (RET) and ISC for a BODIPY/aza-BODIPY based PS.

In a closely related report, Zhao and coworkers summarized the literature pertaining to design approaches for triplet PSs [120]. An example was the design of complexes having large molecular absorptivity values (ε_{max}) in the visible spectrum and long-lived triplet excited states. Energy funneling based triplet PSs that show broadband absorptions in the visible spectrum were discussed, as a way to enhance triplet PS performance. A key goal was to develop new triplet PSs by establishing correlations between ISC and molecular structures. This report included Ru(II) polyimine triplet PSs structures such as the coumarin-based Ru(II) complex in Figure 30, which gave an absorption at 341 nm having $\varepsilon_{max} \sim 79,000$ *versus* an $\varepsilon_{max} = 14,000$ when the coumarin moiety was replaced by *N*-acetyl group. It was shown that the energy level of the ligand localized excited state (^{1}IL) was higher than the ^{1}MLCT (metal to ligand charge transfer) state, providing efficient energy transfer or internal conversion from the coumarin moiety to the coordination center. In addition, the energy level of the ^{3}IL of coumarin is significantly higher than the ^{3}MLCT; consequently the phosphorescence lifetime and the quantum yield were not adversely affected by the ligand.
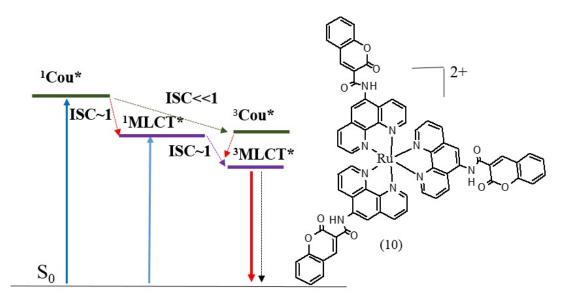
Figure 30. Energy level diagram showing Ru(II) complex having a light-harvesting coumarin ligand.

Ru(II) complexes having pyrene and naphthalimide appendages were also reported [120,124,125]. Attachment of pyrene groups to the phenanthroline (Phen) ligand led to enhancement of the absorption in the 300–350 nm region. In this case, the ^{3}IL energy level is close to the ^{3}MLCT and the triplet state lifetime is enhanced. Similarly, a long lived triplet state was observed for the Ru(II) polyimine complex having a 4-piperidinyl-1,8-naphthalimide group attached to the Phen ligand (Figure 31).

Another approach to increasing the triplet lifetime involved having the ligand and coordination center connected through π conjugation such as a C≡C moiety [120,122]. The properly chosen ligand can also enhance λ_{max} but the ligand cannot be very bulky since this would decrease ISC efficiency.

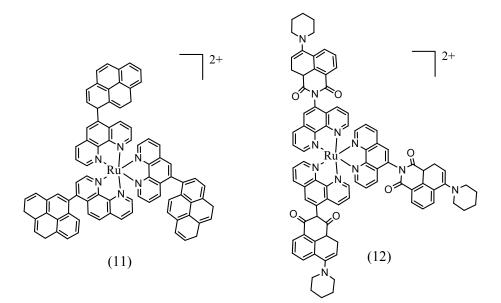**Figure 31.** Example Ru(II) based phen complexes having close ^{3}MLCT and ^{3}IL states.

Figure 32 shows that the ^{3}MLCT state of the coordination center (1.94 eV) is higher than the ^{3}IL state energy level of Bodipy (1.72 eV). Therefore the phosphorescence of the ^{3}MLCT state is quenched by ^{3}MLCT→^{3}IL and the triplet state is mostly localized on the Bodipy unit. In this case, energy transfer

from ^{1}IL→^{1}MLCT is not likely to happen since the ^{1}IL is located below ^{1}MLCT. Therefore the strong visible absorptions of the Bodipy (523 nm) and ε$_{max}$ (66,000) do not aid triplet excited state production.
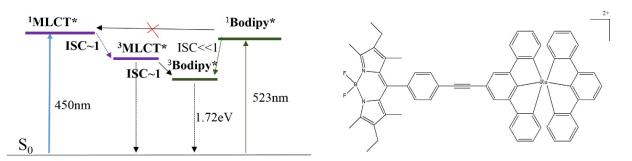

Figure 32. Energy diagram for a Ru(II) complex having BODIPY as a visible light harvesting ligand, showing energy transfer is unlikely.

It is known that charge transfer can decrease ^{1}O$_2$ production by quenching of the excited state [126]. However, complexes such as Ru(II) bipyridine and related compounds are good PSs of singlet oxygen in spite of the charge transfer (CT) nature of the lowest excited state of these compounds. This is because of the relatively long lifetime of the triplet metal-to-ligand charge transfer states, ^{3}MLCT, of many Ru(II) coordination compounds that make these excited states susceptible to quenching by oxygen. It is been reported that the MLCT absorption mainly produces ^{1}MLCT that undergo ISC and populate ^{3}MLCT [127].

4. Conclusions

A substantial number of porphyrinoid and non-porphyrinoid PSs both hydrophobic and hydrophilic have been published, some of which show promise as PDT agents. The key goal of much of this work was to identify approaches to PSs having high selectivity for tumors than healthy tissues and/or enhance ^{1}O$_2$ production. In results strictly comparing the advantages and disadvantages of hydrophobic *vs* hydrophilic PS dyes, is appears that amphiphilic PSs provide the way forward in this area. To increase the selectivity of PSs for malignant tissues, the use of PS-nanoparticle combinations has provided an interesting and potentially viable approach. In this regard, micelles/polymeric micelles having the ability to transport hydrophobic and amphiphilic PSs to mitochondria have been developed. To increase ^{1}O$_2$ production, systems containing heavy atoms and having enhanced ISC and two-photon absorption properties are of considerable interest. Notably, the PDT field has attracted photochemists, organic and inorganic chemists, color chemists, pharmacologists, and more recently, laser technologists, among others, to this still fascinating opportunity to have an effective, non-invasive resource for cancer treatment.

Author Contributions

This review was written by Nahid Mehraban, in partial fulfillment of the requirements for her PhD degree, under the direction of Harold S. Freeman.

Conflicts of Interest

The authors declare no conflict of interest.

References

1. Dougherty, T.J.; Gomer, C.J.; Henderson, B.W.; Jori, G.; Kessel, D.; Korbelik, M.; Moan, J.; Peng, Q. Photodynamic therapy. *J. Natl. Cancer Inst.* **1998**, *90*, 889–905.
2. Wainwright, M. Non-porphyrin photosensitizers in biomedicine. *Chem. Soc. Rev.* **1996**, *25*, 351–359.
3. Yoon, I.; Li, J.Z.; Shim, Y.K. Advance in photosensitizers and light delivery for photodynamic therapy. *Clin. Endosc.* **2013**, *46*, 7–23.
4. Ormond, A.B.; Freeman, H.S. Dye sensitizers for photodynamic therapy. *Materials* **2013**, *6*, 817–840.
5. Wainwright, M. Photodynamic therapy–from dyestuffs to high–tech clinical practice. *Rev. Prog. Colorat. Relat. Top.* **2004**, *34*, 95–109.
6. De Melo, L.S.; Gomes, A.S.; Saska, S.; Nigoghossian, K.; Messaddeq, Y.; Ribeiro, S.J.; de Araujo, R.E. Singlet oxygen generation enhanced by silver-pectin nanoparticles. *J. Fluoresc.* **2012**, *22*, 1633–1638.
7. Zhu, T.C.; Finlay, J.C. The role of photodynamic therapy (PDT) physics. *Med. Phys.* **2008**, *35*, 3127–3136.
8. Kamkaew, A.; Lim, S.H.; Lee, H.B.; Kiew, L.V.; Chung, L.Y.; Burgess, K. BODIPY dyes in photodynamic therapy. *Chem. Soc. Rev.* **2013**, *42*, 77–88.
9. Avirah, R.R.; Jayaram, D.T.; Adarsh, N.; Ramaiah, D. Squaraine dyes in PDT: From basic design to *in vivo* demonstration. *Org. Biomol. Chem.* **2012**, *10*, 911–920.
10. Dąbrowski, J.M.; Urbanska, K.; Arnaut, L.G.; Pereira, M.M.; Abreu, A.R.; Simões, S.; Stochel, G. Biodistribution and Photodynamic Efficacy of a Water-Soluble, Stable, Halogenated Bacteriochlorin against Melanoma. *ChemMedChem* **2011**, *6*, 465–475.
11. Maggioni, D.; Galli, M.; D'Alfonso, L.; Inverso, D.; Dozzi, M.V.; Sironi, L.; Iannacone, M.; Collini, M.; Ferruti, P.; Ranucci, E. A Luminescent Poly (amidoamine)–Iridium Complex as a New Singlet-Oxygen Sensitizer for Photodynamic Therapy. *Inorg. Chem.* **2015**, *54*, 544–553.
12. Ogilby, P.R. Singlet oxygen: There is indeed something new under the sun. *Chem. Soc. Rev.* **2010**, *39*, 3181–3209.
13. Sharpless, C.M.; Blough, N.V. The importance of charge-transfer interactions in determining chromophoric dissolved organic matter (CDOM) optical and photochemical properties. *Environ. Sci.* **2014**, *16*, 654–671.
14. Salice, P.; Arnbjerg, J.; Pedersen, B.W.; Toftegaard, R.; Beverina, L.; Pagani, G.A.; Ogilby, P.R. Photophysics of squaraine dyes: Role of charge-transfer in singlet oxygen production and removal. *J. Physics. Chem. A* **2010**, *114*, 2518–2525.
15. Weyergang, A.; Berg, K.; Kaalhus, O.; Peng, Q.; Selbo, P.K. Photodynamic therapy targets the mTOR signaling network *in vitro* and *in vivo*. *Mol. Pharm.* **2008**, *6*, 255–264.
16. Agostinis, P.; Berg, K.; Cengel, K.A.; Foster, T.H.; Girotti, A.W.; Gollnick, S.O.; Hahn, S.M.; Hamblin, M.R.; Juzeniene, A.; Kessel, D. Photodynamic therapy of cancer: An update. *CA Cancer J. Clin.* **2011**, *61*, 250–281.

17. Da Silva, E.F.; Pedersen, B.W.; Breitenbach, T.; Toftegaard, R.; Kuimova, M.K.; Arnaut, L.G.; Ogilby, P. R. Irradiation-and sensitizer-dependent changes in the lifetime of intracellular singlet oxygen produced in a photosensitized process. *J. Phys. Chem. B* **2011**, *116*, 445–461.

18. Wilkinson, F.; Helman, W.P.; Ross, A.B. Rate constants for the decay and reactions of the lowest electronically excited singlet state of molecular oxygen in solution. An expanded and revised compilation. *J. Phys. Chem. Ref. Data* **1995**, *24*, 663–677.

19. Schweitzer, C.; Schmidt, R. Physical mechanisms of generation and deactivation of singlet oxygen. *Chem. Rev.* **2003**, *103*, 1685–1758.

20. Robertson, C.; Evans, D.H.; Abrahamse, H. Photodynamic therapy (PDT): A short review on cellular mechanisms and cancer research applications for PDT. *J. Photochem. Photobiol. B Biol.* **2009**, *96*, 1–8.

21. Wei, M.; Chen, M.; Chen, K.; Lou, P.; Lin, S.Y.; Hung, S.; Hsiao, M.; Yao, C.; Shieh, M. Autophagy promotes resistance to photodynamic therapy-induced apoptosis selectively in colorectal cancer stem-like cells. *Autophagy* **2014**, *10*, 1179–1192.

22. Dewaele, M.; Maes, H.; Agostinis, P. ROS-mediated mechanisms of Autophagy stimulation and their relevance in cancer therapy. *Autophagy* **2010**, *6*, 838–854.

23. Xu, J.; Gattacceca, F.; Amiji, M. Biodistribution and Pharmacokinetics of EGFR-Targeted Thiolated Gelatin Nanoparticles Following Systemic Administration in Pancreatic Tumor-Bearing Mice. *Mol. Pharm.* **2013**, *10*, 2031–2044.

24. Castano, A.P.; Demidova, T.N.; Hamblin, M.R. Mechanisms in photodynamic therapy: Part three—photosensitizer pharmacokinetics, biodistribution, tumor localization and modes of tumor destruction. *Photodiagnosis Photodyn. Ther.* **2005**, *2*, 91–106.

25. Dumoulin, F. Design and Conception of Photosensitisers. In *Photosensitizers in Medicine, Environment, and Security*; Springer: Dordrecht, The Netherlands; Heidelberg, Germany; London, UK, New York, NY, USA, 2012.

26. Silva, E.F.; Serpa, C.; Dąbrowski, J.M.; Monteiro, C.J.; Formosinho, S.J.; Stochel, G.; Urbanska, K.; Simões, S.; Pereira, M.M.; Arnaut, L.G. Mechanisms of Singlet-Oxygen and Superoxide-Ion Generation by Porphyrins and Bacteriochlorins and their Implications in Photodynamic Therapy. *Chem. A Eur. J.* **2010**, *16*, 9273–9286.

27. Castano, A.P.; Demidova, T.N.; Hamblin, M.R. Mechanisms in photodynamic therapy: Part one—photosensitizers, photochemistry and cellular localization. *Photodiagnosis Photodyn. Ther.* **2004**, *1*, 279–293.

28. Rubio, N.; Fleury, S.P.; Redmond, R.W. Spatial and temporal dynamics of *in vitro* photodynamic cell killing: Extracellular hydrogen peroxide mediates neighbouring cell death. *Photochem. Photobiol. Sci.* **2009**, *8*, 457–464.

29. Kessel, D.; Reiners, J.J. Promotion of Proapoptotic Signals by Lysosomal Photodamage. *Photochem. Photobiol.* **2015**, doi:10.1111/php.12456.

30. Rajaputra, P.; Nkepang, G.; Watley, R.; You, Y. Synthesis and *in vitro* biological evaluation of lipophilic cation conjugated photosensitizers for targeting mitochondria. *Bioorg. Med. Chem.* **2013**, *21*, 379–387.

31. Balaji, B.; Balakrishnan, B.; Perumalla, S.; Karande, A.A.; Chakravarty, A.R. Mitochondria-Targeting Photocytotoxic Ferrocenyl Conjugates of *N*-Alkylpyridinium Salts. *Eur. J. Inorg. Chem.* **2015**, *2015*, 1398–1407.

32. Odeh, A.M.; Craik, J.D.; Ezzeddine, R.; Tovmasyan, A.; Batinic-Haberle, I.; Benov, L.T. Targeting mitochondria by Zn (II) *N*-Alkylpyridylporphyrins: The impact of Compound sub-mitochondrial partition on cell respiration and overall photodynamic efficacy. *PLoS ONE* **2014**, *9*, e108238.

33. Rancan, F.; Wiehe, A.; Nöbel, M.; Senge, M.O.; Omari, S.A.; Böhm, F.; John, M.; Röder, B. Influence of substitutions on asymmetric dihydroxychlorins with regard to intracellular uptake, subcellular localization and photosensitization of Jurkat cells. *J. Photochem. Photobiolo. B Biol.* **2005**, *78*, 17–28.

34. Reiners, J.J.; Agostinis, P.; Berg, K.; Oleinick, N.L.; Kessel, D.H. Assessing Autophagy in the context of photodynamic therapy. *Autophagy* **2010**, *6*, 7–18.

35. Liu, L.; Zhang, Z.; Xing, D. Cell death via mitochondrial apoptotic pathway due to activation of Bax by lysosomal photodamage. *Free Radic. Biol. Med.* **2011**, *51*, 53–68.

36. Xie, H.; Svenmarker, P.; Axelsson, J.; Gräfe, S.; Kyriazi, M.; Bendsoe, N.; Andersson Engels, S.; Svanberg, K. Pharmacokinetic and biodistribution study following systemic administration of Fospeg®—A Pegylated liposomal mTHPC formulation in a murine model. *J. Biophotonics.* **2015**, *8*, 142–152.

37. Pandey, R.K. Recent advances in photodynamic therapy. *J. Porphyrins Phthalocyanines* **2000**, *4*, 368–373.

38. Pavani, C.; Uchoa, A.F.; Oliveira, C.S.; Iamamoto, Y.; Baptista, M.S. Effect of zinc insertion and hydrophobicity on the membrane interactions and PDT activity of porphyrin photosensitizers. *Photochem. Photobiol. Sci.* **2009**, *8*, 233–240.

39. Zhang, X.; Xu, H. Influence of halogenation and aggregation on photosensitizing properties of zinc phthalocyanine (ZnPC). *J. Chem. Soc. Faraday Trans.* **1993**, *89*, 3347–3351.

40. Sakamoto, K.; Kato, T.; Kawaguchi, T.; Ohno-Okumura, E.; Urano, T.; Yamaoka, T.; Suzuki, S.; Cook, M.J. Photosensitizer efficacy of non-peripheral substituted alkylbenzopyridoporphyrazines for photodynamic therapy of cancer. *J. Photochem. Photobiol. A* **2002**, *153*, 245–253.

41. Baek, S.; Na, K. A nano complex of hydrophilic phthalocyanine and polyethylenimine for improved cellular internalization efficiency and phototoxicity. *Colloids Surf. B Biointerfaces* **2013**, *101*, 493–500.

42. Lee, Y.; Cho, H.; Choi, M.; Park, H.; Bang, J.; Lee, S.; Kwon, I.C.; Kim, S. Directed molecular assembly into a biocompatible photosensitizing nanocomplex for locoregional photodynamic therapy. *J. Control Release* **2015**, *209*, 12–19.

43. Çakır, D.; Göksel, M.; Çakır, V.; Durmus, M.; Biyiklioglu, Z.; Kantekin, H. Amphiphilic Zinc Phthalocyanine Photosensitizers: Synthesis, Photophysicochemical Properties and *in vitro* Studies for Photodynamic Therapy. *Dalton Trans.* **2015**, doi:10.1039/C5DT00747J.

44. Jin, Y.; Zhang, X.; Zhang, B.; Kang, H.; Du, L.; Li, M. Nanostructures of an amphiphilic zinc phthalocyanine polymer conjugate for photodynamic therapy of psoriasis. *Colloids Surf. B Biointerfaces* **2015**, *128*, 405–409.

45. Doshi, M.; Krienke, M.; Khederzadeh, S.; Sanchez, H.; Copik, A.; Oyer, J.; Gesquiere, A.J. Conducting Polymer Nanoparticles for Targeted Cancer Therapy. *RSC Adv.* **2015**, *5*, 37943–37956.

46. Lo, P.C.; Huang, J.D.; Cheng, D.Y.Y.; Chan, E.Y.M.; Fong, W.P.; Ko, W.H.; Ng, D.K. P. New amphiphilic silicon (IV) phthalocyanines as efficient photosensitizers for photodynamic therapy: Synthesis, photophysical properties, and *in vitro* photodynamic activities. *Chem. A Eur. J.* **2004**, *10*, 4831–4838.

47. Theodossiou, T.A.; Gonçalves, A.R.; Yannakopoulou, K.; Skarpen, E.; Berg, K. Photochemical Internalization of Tamoxifens Transported by a "Trojan-Horse" Nanoconjugate into Breast-Cancer Cell Lines. *Angew. Chem. Int. Ed.* **2015**, *54*, 4885–4889.

48. Moromizato, S.; Hisamatsu, Y.; Suzuki, T.; Matsuo, Y.; Abe, R.; Aoki, S. Design and synthesis of a luminescent cyclometalated iridium (III) complex having N, *N*-diethylamino group that stains acidic intracellular organelles and induces cell death by photoirradiation. *Inorg. Chem.* **2012**, *51*, 12697–12706.

49. Nakagawa, A.; Hisamatsu, Y.; Moromizato, S.; Kohno, M.; Aoki, S. Synthesis and Photochemical Properties of pH Responsive Tris-Cyclometalated Iridium (III) Complexes That Contain a Pyridine Ring on the 2-Phenylpyridine Ligand. *Inorg. Chem.* **2013**, *53*, 409–422.

50. Huang, P.; Xu, C.; Lin, J.; Wang, C.; Wang, X.; Zhang, C.; Zhou, X.; Guo, S.; Cui, D. Folic Acid-conjugated Graphene Oxide loaded with Photosensitizers for Targeting Photodynamic Therapy. *Theranostics* **2011**, *1*, 240–250.

51. Schneider, R.; Schmitt, F.; Frochot, C.; Fort, Y.; Lourette, N.; Guillemin, F.; Müller, J.; Barberi-Heyob, M. Design, synthesis, and biological evaluation of folic acid targeted tetraphenylporphyrin as novel photosensitizers for selective photodynamic therapy. *Bioorg. Med. Chem.* **2005**, *13*, 2799–2808.

52. Van Dongen, G.A.M.S.; Visser, G.W.M.; Vrouenraets, M.B. Photosensitizer-antibody conjugates for detection and therapy of cancer. *Adv. Drug Deliv. Rev.* **2004**, *56*, 31–52.

53. Josefsen, L.; Boyle, R. Photodynamic therapy: Novel third-generation photosensitizers one step closer? *Br. J. Pharmacol.* **2008**, *154*, 1–3.

54. Wöhrle, D.; Hirth, A.; Bogdahn-Rai, T.; Schnurpfeil, G.; Shopova, M. Photodynamic therapy of cancer: Second and third generations of photosensitizers. *Russ. Chem. Bull.* **1998**, *47*, 807–816.

55. Van Nostrum, C.F. Polymeric micelles to deliver photosensitizers for photodynamic therapy. *Adv. Drug Deliv. Rev.* **2004**, *56*, 9–16.

56. Komeda, C.; Ikeda, A.; Kikuchi, J.; Ishida-Kitagawa, N.; Tatebe, H.; Shiozaki, K.; Akiyama, M. A photo-triggerable drug carrier based on cleavage of PEG lipids by photosensitiser-generated reactive singlet oxygen. *Org. Biomol. Chem.* **2013**, *11*, 2567–2570.

57. Bovis, M.J.; Woodhams, J.H.; Loizidou, M.; Scheglmann, D.; Bown, S.G.; MacRobert, A.J. Improved *in vivo* delivery of m-THPC via pegylated liposomes for use in photodynamic therapy. *J. Control Release* **2012**, *157*, 196–205.

58. Choi, Y.; Kim, S.; Choi, M.; Ryoo, S.; Park, J.; Min, D.; Kim, B. Highly Biocompatible Carbon Nanodots for Simultaneous Bioimaging and Targeted Photodynamic Therapy *in Vitro* and *in Vivo*. *Adv. Funct. Mater.* **2014**, *24*, 5781–5789.

59. Castagnos, P.; Siqueira-Moura, M.; Goto, P.L.; Perez, E.; Franceschi, S.; Rico-Lattes, I.; Tedesco, A.; Blanzat, M. Catanionic vesicles charged with chloroaluminium phthalocyanine for topical photodynamic therapy. *In vitro* phototoxicity towards human carcinoma and melanoma cell lines. *RSC Adv.* **2014**, *4*, 39372–39377.

60. Wang, N.; Zhao, Z.; Lv, Y.; Fan, H.; Bai, H.; Meng, H.; Long, Y.; Fu, T.; Zhang, X.; Tan, W. Gold nanorod-photosensitizer conjugate with extracellular pH-driven tumor targeting ability for photothermal/photodynamic therapy. **2014**, *7*, 1291–1301.

61. Cheng, Y.; Doane, T.L.; Chuang, C.; Ziady, A.; Burda, C. Near Infrared Light-Triggered Drug Generation and Release from Gold Nanoparticle Carriers for Photodynamic Therapy. *Small* **2014**, *10*, 1799–1804.

62. Fraix, A.; Gref, R.; Sortino, S. A multi-photoresponsive supramolecular hydrogel with dual-color fluorescence and dual-modal photodynamic action. *J. Mater. Chem. B* **2014**, *2*, 3443–3449.

63. Kesharwani, P.; Jain, K.; Jain, N. K. Dendrimer as nanocarrier for drug delivery. *Prog. Polym. Sci.* **2014**, *39*, 268–307.

64. Yin, M.; Ju, E.; Chen, Z.; Li, Z.; Ren, J.; Qu, X. Upconverting Nanoparticles with a Mesoporous TiO2 Shell for Near-Infrared-Triggered Drug Delivery and Synergistic Targeted Cancer Therapy. *Chem. A Eur. J.* **2014**, *20*, 14012–14017.

65. García Vior, M.C.; Marino, J.; Roguin, L.P.; Sosnik, A.; Awruch, J. Photodynamic Effects of Zinc (II) Phthalocyanine-Loaded Polymeric Micelles in Human Nasopharynx KB Carcinoma Cells. *Photochem. Photobiol.* **2013**, *89*, 492–500.

66. Chen, Y.; Lo, C.; Hsiue, G. Multifunctional nanomicellar systems for delivering anticancer drugs. *J. Biomed. Mate Res. Part A* **2014**, *102*, 2024–2038.

67. Kataoka, K.; Harada, A.; Nagasaki, Y. Block copolymer micelles for drug delivery: Design, characterization and biological significance. *Adv. Drug Deliv. Rev.* **2001**, *47*, 113–131.

68. Peng, C.; Shieh, M.; Tsai, M.; Chang, C.; Lai, P. Self-assembled star-shaped chlorin-core poly(ε-caprolactone)–poly(ethylene glycol) diblock copolymer micelles for dual chemo-photodynamic therapies. *Biomaterials* **2008**, *29*, 3599–3608.

69. Wu, D.; Li, Z.; Li, C.; Fan, J.; Lu, B.; Chang, C.; Cheng, S.; Zhang, X.; Zhuo, R. Porphyrin and galactosyl conjugated micelles for targeting photodynamic therapy. *Pharm. Res.* **2010**, *27*, 187–199.

70. Knop, K.; Mingotaud, A.; El-Akra, N.; Violleau, F.; Souchard, J. Monomeric pheophorbide (a)-containing poly (ethyleneglycol-b-ε-caprolactone) micelles for photodynamic therapy. *Photochem. Photobiol. Sci.* **2009**, *8*, 396–404.

71. Synatschke, C.V.; Nomoto, T.; Cabral, H.; Förtsch, M.; Toh, K.; Matsumoto, Y.; Miyazaki, K.; Hanisch, A.; Schacher, F.H.; Kishimura, A. Multicompartment Micelles with Adjustable Poly (ethylene glycol) Shell for Efficient *in Vivo* Photodynamic Therapy. *ACS Nano* **2014**, *8*, 1161–1172.

72. Ma, D.; Liu, Z.; Zheng, Q.; Zhou, X.; Zhang, Y.; Shi, Y.; Lin, J.; Xue, W. Star-Shaped Polymer Consisting of a Porphyrin Core and Poly (L-lysine) Dendron Arms: Synthesis, Drug Delivery, and *In Vitro* Chemo/Photodynamic Therapy. *Macromol. Rapid Commun.* **2013**, *34*, 548–552.

73. Lee, S.U.; Min, K.H.; Jeong, S.Y.; Bae, H.; Lee, S.C. Calcium phosphate-reinforced photosensitizer-loaded polymer nanoparticles for photodynamic therapy. *Chem. Asian J.* **2013**, *8*, 3222–3229.

74. Li, S.P.; Lau, C.T.; Louie, M.; Lam, Y.; Cheng, S.H.; Lo, K.K. Mitochondria-targeting cyclometalated iridium (III)–PEG complexes with tunable photodynamic activity. *Biomaterials* **2013**, *34*, 7519–7532.

75. Verma, S.; Watt, G.M.; Mai, Z.; Hasan, T. Strategies for Enhanced Photodynamic Therapy Effects. *Photochem. Photobiol.* **2007**, *83*, 996–1005.

76. Master, A.; Malamas, A.; Solanki, R.; Clausen, D.M.; Eiseman, J.L.; Sen Gupta, A. A cell-targeted photodynamic nanomedicine strategy for head and neck cancers. *Mol. Pharm.* **2013**, *10*, 1988–1997.

77. Peng, C.; Lai, P.; Lin, F.; Yueh-Hsiu Wu, S.; Shieh, M. Dual chemotherapy and photodynamic therapy in an HT-29 human colon cancer xenograft model using SN-38-loaded chlorin-core star block copolymer micelles. *Biomaterials* **2009**, *30*, 3614–3625.

78. Koo, H.; Lee, H.; Lee, S.; Min, K.H.; Kim, M.S.; Lee, D.S.; Choi, Y.; Kwon, I.C.; Kim, K.; Jeong, S.Y. *In vivo* tumor diagnosis and photodynamic therapy via tumoral pH-responsive polymeric micelles. *Chem. Commun.* **2010**, *46*, 5668–5670.

79. Lau, J.T.; Lo, P.; Jiang, X.; Wang, Q.; Ng, D.K. A Dual Activatable Photosensitizer toward Targeted Photodynamic Therapy. *J. Med. Chem.* **2014**, *57*, 4088–4097.

80. Liang, J.; Wu, W.; Xu, X.; Zhuo, R.; Zhang, X. pH Responsive micelle self-assembled from a new amphiphilic peptide as anti-tumor drug carrier. *Colloids Surf. B Biointerfaces* **2014**, *114*, 398–403.

81. Master, A.M.; Qi,Y.; Oleinick, N.L.; Gupta, A.S. EGFR-mediated intracellular delivery of Pc 4 nanoformulation for targeted photodynamic therapy of cancer: *In vitro* studies. *Nanomedicine* **2012**, *8*, 655–664.

82. Li, L.; Cho, H.; Yoon, K.H.; Kang, H.C.; Huh, K.M. Antioxidant-photosensitizer dual-loaded polymeric micelles with controllable production of reactive oxygen species. *Int. J. Pharm.* **2014**, *471*, 339–348.

83. Hofman, J.; Carstens, M.G.; van Zeeland, F.; Helwig, C.; Flesch, F.M.; Hennink, W.E.; Van Nostrum, C.F. Photocytotoxicity of mTHPC (temoporfin) loaded polymeric micelles mediated by lipase catalyzed degradation. *Pharm. Res.* **2008**, *25*, 2065–2073.

84. Chen, J.; Wang, H.; Li, C.; Han, K.; Zhang, X.; Zhuo, R. Construction of surfactant-like tetra-tail amphiphilic peptide with RGD ligand for encapsulation of porphyrin for photodynamic therapy. *Biomaterials* **2011**, *32*, 1678–1684.

85. Ding, H.; Sumer, B.D.; Kessinger, C.W.; Dong, Y.; Huang, G.; Boothman, D.A.; Gao, J. Nanoscopic micelle delivery improves the photophysical properties and efficacy of photodynamic therapy of protoporphyrin IX. *J. Control Release* **2011**, *151*, 271–277.

86. Yuan, A.; Yang, B.; Wu, J.; Hu, Y.; Ming, X. Dendritic nanoconjugates of photosensitizer for targeted photodynamic therapy. *Acta Biomate.* **2015**, *21*, 63–73.

87. Dong, H.; Li, Y.; Wen, H.; Xu, M.; Liu, L.; Li, Z.; Guo, F.; Shi, D. Highly Efficient Drug Delivery Nanosystem via L-Phenylalanine Triggering Based on Supramolecular Polymer Micelles. *Macromol. Rapid Commun.* **2011**, *32*, 540–545.

88. Mojzisova, H.; Bonneau, S.; Vever-Bizet, C.; Brault, D. The pH-dependent distribution of the photosensitizer chlorin e6 among plasma proteins and membranes: A physico-chemical approach. *Biochim. Biophys. Acta* **2007**, *1768*, 366–374.

89. Chong, K.; Ku, T.; Saw, P.E.; Jon, S.; Park, J.; Choi, C. Enhancement of the photocytotoxic efficiency of sub-12 nm therapeutic polymeric micelles with increased co-localisation in mitochondria. *Chem. Commun.* **2013**, *49*, 11476–11478.

90. Nishiyama, N.; Nakagishi, Y.; Morimoto, Y.; Lai, P.; Miyazaki, K.; Urano, K.; Horie, S.; Kumagai, M.; Fukushima, S.; Cheng, Y. Enhanced photodynamic cancer treatment by supramolecular nanocarriers charged with dendrimer phthalocyanine. *J. Control Release* **2009**, *133*, 245–251.

91. Master, A.M.; Livingston, M.; Oleinick, N.L.; Sen Gupta, A. Optimization of a nanomedicine-based silicon Phthalocyanine 4 Photodynamic Therapy (Pc 4-PDT) strategy for targeted treatment of EGFR-overexpressing cancers. *Mol. Pharm.* **2012**, *9*, 2331–2338.

92. Syu, W.; Yu, H.; Hsu, C.; Rajan, Y.C.; Hsu, Y.; Chang, Y.; Hsieh, W.; Wang, C.; Lai, P. Improved Photodynamic Cancer Treatment by Folate-Conjugated Polymeric Micelles in a KB Xenografted Animal Model. *Small* **2012**, *8*, 2060–2069.

93. Gong, H.; Dong, Z.; Liu, Y.; Yin, S.; Cheng, L.; Xi, W.; Xiang, J.; Liu, K.; Li, Y.; Liu, Z. Engineering of Multifunctional Nano-Micelles for Combined Photothermal and Photodynamic Therapy under the Guidance of Multimodal Imaging. *Adv. Funct. Mater.* **2014**, *24*, 6492–6502.

94. Lee, U.Y.; Oh, Y.T.; Kim, D.; Lee, E.S. Multimeric grain-marked micelles for highly efficient photodynamic therapy and magnetic resonance imaging of tumors. *Int. J. Pharm.* **2014**, *471*, 166–172.

95. Pellosi, D.S.; Estevão, B.M.; Freitas, C.F.; Tsubone, T.M.; Caetano, W.; Hioka, N. Photophysical properties of erythrosin ester derivatives in ionic and non-ionic micelles. *Dyes Pigm.* **2013**, *99*, 705–712.

96. Chen, K.; Yu, M.; Zhang, H.; Ma, D.; Pang, S.; Huang, W.; Peng, Y. In polyion complex micelles incorporating poly (aryl benzyl ether) dendritic phthalocyanine: Effective photosensitizers for enhanced photodynamic therapy. *Proc. SPIE* **2012**, doi:10.1117/12.2001194.

97. Gibot, L.; Lemelle, A.; Till, U.; Moukarzel, B.; Mingotaud, A.; Pimienta, V.; Saint-Aguet, P.; Rols, M.; Gaucher, M.; Violleau, F. Polymeric micelles encapsulating photosensitizer: Structure/photodynamic therapy efficiency relation. *Biomacromolecules* **2014**, *15*, 1443–1455.

98. Shao, W.; Wang, H.; He, S.; Shi, L.; Peng, K.; Lin, Y.; Zhang, L.; Ji, L.; Liu, H. Photophysical properties and singlet oxygen generation of three sets of halogenated corroles. *J. Phys. Chem. B* **2012**, *116*, 14228–14234.

99. Lo, P.; Wang, S.; Zeug, A.; Meyer, M.; Röder, B.; Ng, D.K.P. Preparation and photophysical properties of halogenated silicon(IV) phthalocyanines substituted axially with poly(ethylene glycol) chains. *Tetrahedron Lett.* **2003**, *44*, 1967–1970.

100. Tanielian, C.; Wolff, C. Determination of the parameters controlling singlet oxygen production via oxygen and heavy-atom enhancement of triplet yields. *J. Phys. Chem.* **1995**, *99*, 9831–9837.

101. De Melo, J.; Rondão, R.; Burrows, H.D.; Melo, M.J.; Navaratnam, S.; Edge, R.; Voss, G. Spectral and photophysical studies of substituted indigo derivatives in their keto forms. *ChemPhysChem.* **2006**, *7*, 2303–2311.

102. Gaboury, L.; Giasson, R.; Gupta, A.K.; Li, T.; Villeneuve, L. WO1996007431 A1, 14 March 1996.

103. Araki, K.; Engelmann, F.M.; Mayer, I.; Toma, H.E.; Baptista, M.S.; Maeda, H.; Osuka, A.; Furuta, H. Doubly *N*-Confused Porphyrins as Efficient Sensitizers for Singlet Oxygen Generation. *Chem. Lett.* **2003**, *32*, 244–245.

104. Obata, M.; Hirohara, S.; Tanaka, R.; Kinoshita, I.; Ohkubo, K.; Fukuzumi, S.; Tanihara, M.; Yano, S. *In vitro* heavy-atom effect of palladium (II) and platinum (II) complexes of pyrrolidine-fused chlorin in photodynamic therapy. *J. Med. Chem.* **2009**, *52*, 2747–2753.

105. Weitman, H.; Shatz, S.; Ehrenberg, B. Complexation of Mg-tetrabenzoporphyrin with pyridine enhances singlet oxygen generation and affects its partitioning into apolar microenvironments. *J. Photochem. Photobiol. A* **2009**, *203*, 7–12.

106. Marydasan, B.; Nair, A.K.; Ramaiah, D. Optimization of Triplet Excited State and Singlet Oxygen Quantum Yields of Picolylamine–Porphyrin Conjugates through Zinc Insertion. *J. Phys. Chem. B* **2013**, *117*, 13515–13522.

107. Peceli, D.; Hu, H.; Fishman, D.A.; Webster, S.; Przhonska, O.V.; Kurdyukov, V.V.; Slominsky, Y.L.; Tolmachev, A.I.; Kachkovski, A.D.; Gerasov, A.O. Enhanced Intersystem Crossing Rate in Polymethine-Like Molecules: Sulfur-Containing Squaraines *versus* Oxygen-Containing Analogues. *J. Physics. Chem. A* **2013**, *117*, 2333–2346.

108. Webster, S.; Peceli, D.; Hu, H.; Padilha, L.A.; Przhonska, O.V.; Masunov, A.E.; Gerasov, A.O.; Kachkovski, A.D.; Slominsky, Y.L.; Tolmachev, A.I. Near-unity quantum yields for intersystem crossing and singlet oxygen generation in polymethine-like molecules: Design and experimental realization. *J. Phys. Chem. Lett.* **2010**, *1*, 2354–2360.

109. Sagun, E.; Zenkevich, E.; Knyukshto, V.; Panarin, A.Y.; Semeikin, A.; Lyubimova, T. Relaxation processes with participation of excited S 1 and T 1 states of spatially distorted meso-phenyl-substituted octamethylporphyrins. *Opt. Spectrosc.* **2012**, *113*, 388–400.

110. Röder, B.; Büchner, M.; Rückmann, I.; Senge, M.O. Correlation of photophysical parameters with macrocycle distortion in porphyrins with graded degree of saddle distortion. *Photochem. Photobiol. Sci.* **2010**, *9*, 1152–1158.

111. Shimakoshi, H.; Baba, T.; Iseki, Y.; Aritome, I.; Endo, A.; Adachi, C.; Hisaeda, Y. Photophysical and photosensitizing properties of brominated porphycenes. *Chem. Commun.* **2008**, *2008*, 2882–2884.

112. Luo, C.; Zhou, Q.; Jiang, G.; He, L.; Zhang, B.; Wang, X. The synthesis and $^1O_2$ photosensitization of halogenated asymmetric aniline-based squaraines. *New J. Chem.* **2011**, *35*, 1128–1132.

113. Zhou, L.; Wei, S.; Ge, X.; Zhou, J.; Yu, B.; Shen, J. External heavy-atomic construction of photosensitizer nanoparticles for enhanced *in vitro* photodynamic therapy of cancer. *J. Phys. Chem. B* **2012**, *116*, 12744–12749.

114. Maeda, D.; Shimakoshi, H.; Abe, M.; Hisaeda, Y. Syntheses and photophysical behavior of porphyrin isomer Sn (IV) complexes. *Inorg. Chem.* **2009**, *48*, 9853–9860.

115. Kim, O.; Lee, K.; Woo, H.Y.; Kim, K.; He, G.S.; Swiatkiewicz, J.; Prasad, P.N. New class of two-photon-absorbing chromophores based on dithienothiophene. *Chem. Mater.* **2000**, *12*, 284–286.

116. Das, S.; Nag, A.; Goswami, D.; Bharadwaj, P.K. Zinc (II)-and copper (I)-mediated large two-photon absorption cross sections in a bis-cinnamaldiminato Schiff base. *J. Am. Chem. Soc.* **2006**, *128*, 402–403.

117. Oar, M.A.; Dichtel, W.R.; Serin, J.M.; Fréchet, J.M.; Rogers, J.E.; Slagle, J.E.; Fleitz, P.A.; Tan, L.; Ohulchanskyy, T.Y.; Prasad, P.N. Light-harvesting chromophores with metalated porphyrin cores for tuned photosensitization of singlet oxygen via two-photon excited FRET. *Chem. Mater.* **2006**, *18*, 3682–3692.

118. Luo, T.; Wilson, B.C.; Lu, Q. Evaluation of one- and two-photon activated photodynamic therapy with pyropheophorbide-a methyl ester in human cervical, lung and ovarian cancer cells. *J. Photochem. Photobiol. B Biol.* **2014**, *132*, 102–110.

119. Pefkianakis, E.K.; Christodouleas, D.; Giokas, D.L.; Papadopoulos, K.; Vougioukalakis, G.C.A Family of RuII Photosensitizers with High Singlet Oxygen Quantum Yield: Synthesis, Characterization, and Evaluation. *Eur. J. Inorg. Chem.* **2013**, *2013*, 4628–4635.

120. Zhao, J.; Wu, W.; Sun, J.; Guo, S. Triplet photosensitizers: From molecular design to applications. *Chem. Soc. Rev.* **2013**, *42*, 5323–5351.

121. Zhao, Q.; Liu, S.; Shi, M.; Li, F.; Jing, H.; Yi, T.; Huang, C. Tuning photophysical and electrochemical properties of cationic iridium (III) complex salts with imidazolyl substituents by proton and anions. *Organometallics* **2007**, *26*, 5922–5930.

122. Majumdar, P.; Yuan, X.; Li, S.; Le Guennic, B.; Ma, J.; Zhang, C.; Jacquemin, D.; Zhao, J. Cyclometalated Ir (III) complexes with styryl-BODIPY ligands showing near IR absorption/emission: Preparation, study of photophysical properties and application as photodynamic/luminescence imaging materials. *J. Mater. Chem. B* **2014**, *2*, 2838–2854.

123. Guo, S.; Ma, L.; Zhao, J.; Küçüköz, B.; Karatay, A.; Hayvali, M.; Yaglioglu, H.G.; Elmali, A. BODIPY triads triplet photosensitizers enhanced with intramolecular resonance energy transfer (RET): Broadband visible light absorption and application in photooxidation. *Chem. Sci.* **2014**, *5*, 489–500.

124. Armaroli, N. Electronic Excited-State Engineering. *ChemPhysChem* **2008**, *9*, 371–373.

125. Tyson, D.S.; Luman, C.R.; Zhou, X.; Castellano, F.N. New Ru (II) chromophores with extended excited-state lifetimes. *Inorg. Chem.* **2001**, *40*, 4063–4071.

126. Vachova, L.; Novakova, V.; Kopecky, K.; Miletin, M.; Zimcik, P. Effect of intramolecular charge transfer on fluorescence and singlet oxygen production of phthalocyanine analogues. *Dalton Trans.* **2012**, *41*, 11651–11656.

127. Abdel-Shafi, A.A.; Hassanin, H.A.; Al-Shihry, S.S. Partial charge transfer contribution to the solvent isotope effect and photosensitized generation of singlet oxygen, O_2 ($^1\Delta_g$), by substituted ruthenium (II) bipyridyl complexes in aqueous media. *Photochem. Photobiol. Sci.* **2014**, *13*, 1330–1337.